Journal of Loss Prevention in the Process Industries 71 (2021) 104484

Contents lists available at ScienceDirect

Journal of Loss Prevention in the Process Industries

journal homepage: http://www.elsevier.com/locate/jlp

Effect of turbulence spatial distribution on the deflagration index: Comparison between 20 L and 1 m^3 vessels

Maria Portarapillo [a,*], Roberto Sanchirico [b], Almerinda Di Benedetto [a]

[a] Department of Chemical, Materials and Production Engineering, University of Naples Federico II Naples, 80125, Italy
[b] Institute for Research on Combustion-CNR, Naples, 80125, Italy

ARTICLE INFO

Keywords:
Process safety
Dust explosion
Standard equipment
Turbulence
CFD simulations

ABSTRACT

In this work, the effect of spatial distribution and values of the turbulent kinetic energy on the pressure-time history and then on the explosion parameters (deflagration index and maximum pressure) was quantified in both the standard vessels (20 L and 1 m^3).

The turbulent kinetic energy maps were computed in both 20 L and 1 m^3 vessels by means of CFD simulations with validated models. Starting from these maps, the turbulent flame propagation of cornstarch was calculated, by means of the software CHEMKIN. Then, the pressure-time history was evaluated and from this, the explosion parameters.

Calculations were performed for three cases: not uniform turbulence level as computed from CFD simulations, uniform turbulence level and equal to the maximum value, uniform profile and equal to the minimum value. It was found that the cornstarch in the 20 L vessel get variable classes (St-1, St-2, St-3) with respect to the 1 m^3 (St-1). However, simulations performed on increasing the ignition delay time, shown that the same results can be attained only using 260 ms as ignition delay time in the 20 L vessel.

1. Introduction

Due to the high number of accidents in industrial chemical processes due to explosions of combustible dusts, dust mixtures, and hybrid mixtures, the evaluation of the flammability and explosion parameters of dusts is mandatory (Dust Safety Science, 2020). Such parameters are measured in standard vessels, according to standard procedures (ASTM E1226-19, 2019; ASTM E1515-14, 1993; ASTM E2931-13, 2013; BS EN 14034-1, 2004; ISO 6184–1:1985, 1985). The vessels used for the explosion parameter measurements are generally the 20 L and the 1 m^3 vessels. A great effort has been devoted to the identification of the conditions at which the results obtained in both vessels are the same. It has been established that, if the same turbulence level is attained before ignition, the measurements in the two vessels are equivalent. Turbulence is generated due to the dust dispersion process: the dust is dispersed into the 20 L sphere from a pressurized dust storage chamber (V = 0.6 L) at 20 barg by means of an outlet valve and a perforated annular nozzle. A time-decaying turbulent flow field is established. Consequently, the initial turbulence level (i.e., turbulence at the moment of ignition) depends significantly on the ignition delay time (t_d), defined as the delay between the onset of dust dispersion and the activation of the ignition source. According to the standard procedures, if in the 20 L sphere the ignition delay time is equal to (60 ± 5) ms, measurements are equivalent to those obtained in the 1 m^3 vessel at ignition delay time equal to (600 ± 100) ms (ASTM E1226-19, 2019; BS EN 14034-1, 2004). However, in the literature, significant discrepancies were found between the results obtained with the 20 L sphere and the 1 m^3 vessel, once dusts different from the reference ones (e.g., lycopodium) are tested. In the case of organic dusts, it was found that dusts weakly reactive in the 20 L sphere are totally not explosible in the 1 m^3 vessel. This effect was attributed to overdriving due to pre-heating/ignition phenomena leading to false positives in smaller explosion chambers (Cashdollar and Chatrathi, 1992; Di Benedetto et al., 2012; Going et al., 2000; Proust et al., 2007; Rodgers and Ural, 2011). In the case of metal dusts, measurements of K_{St} values in the 1 m^3 vessel led to more severe values when compared to the data measured in the 20 L sphere (Clouthier et al., 2019; Taveau et al, 2018, 2019). For this reason, NFPA 68 recommends to measure the explosion severity of the most reactive metal dusts in a 1 m^3 chamber (NFPA, 2018). This finding were attributed to the effect of thermal radiation (Taveau et al., 2019). In addition to all these phenomena, we have recently showed that after injecting dust-air mixtures into the vessels the fluid flow which

* Corresponding author.
E-mail address: maria.portarapillo@unina.it (M. Portarapillo).

https://doi.org/10.1016/j.jlp.2021.104484
Received 19 December 2020; Received in revised form 21 March 2021; Accepted 24 March 2021
Available online 31 March 2021

establishes in the 20 L and in the 1 m^3 vessels is significantly different, even if the recommended ignition delay time is chosen ((60 ± 5) ms in the 20 L vessel, (600 ± 100) ms in the 1 m^3 vessel) (Portarapillo et al., 2020). In particular, we have shown that in the 20 L vessel, the turbulent kinetic energy is much higher and rather not uniform compared to that of 1 m^3 vessel. It has been shown that the same results may be deduced from turbulence measurements (Dahoe et al., 2002; Hauert and Vogl, 1995; Pu et al., 1991; van der Wel et al., 1992; Zhen and Leuckel, 1996). It is worth noting that the preignition turbulence may play a major role in affecting the pressure-time history and the explosion parameter values. As a result, the control of the turbulence level in both vessels is of primary importance in order to have equivalent and reliable measurements (Cashdollar and Chatrathi, 1992; Di Benedetto et al., 2012). In this work, we aim at quantifying the effect of spatial distribution and values of the turbulent kinetic energy on the explosion parameters (deflagration index and maximum pressure). Starting from the turbulent kinetic energy maps as computed in both 20 L and 1 m^3 vessels, we calculated the pressure-time history and from this the explosion parameters. To highlight the effect of the turbulence level homogeneity inside the vessels on the explosion parameters evaluation, the calculations will be carried out in three cases: variable turbulence, maximum turbulence (as computed in the centre of the vessels) and minimum turbulence (found close to the wall). The variability of the explosion parameters between the three cases for each vessel will be indicative of the turbulence level in the vessel and its uniformity. In particular, the smaller the explosion parameters variation between the three cases described, the more homogeneous the turbulence flow field and the less influenced by the properties of the dust. Consequently, in this case, the measurements will be more reliable and repeatable.

2. Description of the methodology

The maximum explosion pressure P_{max} (bar) and the deflagration index K_{St} (bar m/s) were calculated starting from the pressure-time history. In the following the procedure for the calculation of the pressure time histories in the explosion vessel is described.

The steps of the procedure are based on the calculation of:

1. turbulent kinetic energy
2. turbulent burning velocity
3. pressure-time history

In the following sections, each step is described.

2.1. Turbulent kinetic energy

To get the map of the turbulent kinetic energy, we performed CFD simulations of the temporal evolution of fluid dynamic conditions in both vessels (20 L and 1 m^3) by means of a previously developed and validated models (Di Benedetto et al., 2013; Portarapillo et al., 2020). Computations were performed for cornstarch with density and diameter equal to 1500 kg/m^3 and 14 μm, respectively. The choice of the dust was made since the availability of literature data. From the computed maps of the turbulent kinetic energy k (m^2/s^2), the maps of the velocity fluctuation u' (m/s) have been calculated using Equation (1).

$$k = \frac{3}{2}(u')^2 \tag{1}$$

In the following figures, computed maps of the turbulent kinetic energy (a) and of the velocity fluctuations (b) for the 20 L (Fig. 1) and for the 1 m^3 vessel (Fig. 2) are shown.

2.2. Turbulent burning velocity

The turbulent burning velocity S_t (m/s) has to be calculated as function of the velocity fluctuation u' (m/s). Several formulas are available which correlate S_t to u', for both gas and dust flame propagation. In a previous paper (Garcia Agreda et al., 2011), we showed that the relation which better fits the effect of turbulence on S_t is that proposed by Pocheau (Equation (2)) (Pocheau, 1994):

$$S_t = S_l \cdot \left(1 + \left(\frac{u'}{S_l}\right)^2\right)^{0.5} \tag{2}$$

where S_l (m/s) is the laminar burning velocity. The value of the laminar burning velocity was calculated by simulating the flame propagation of

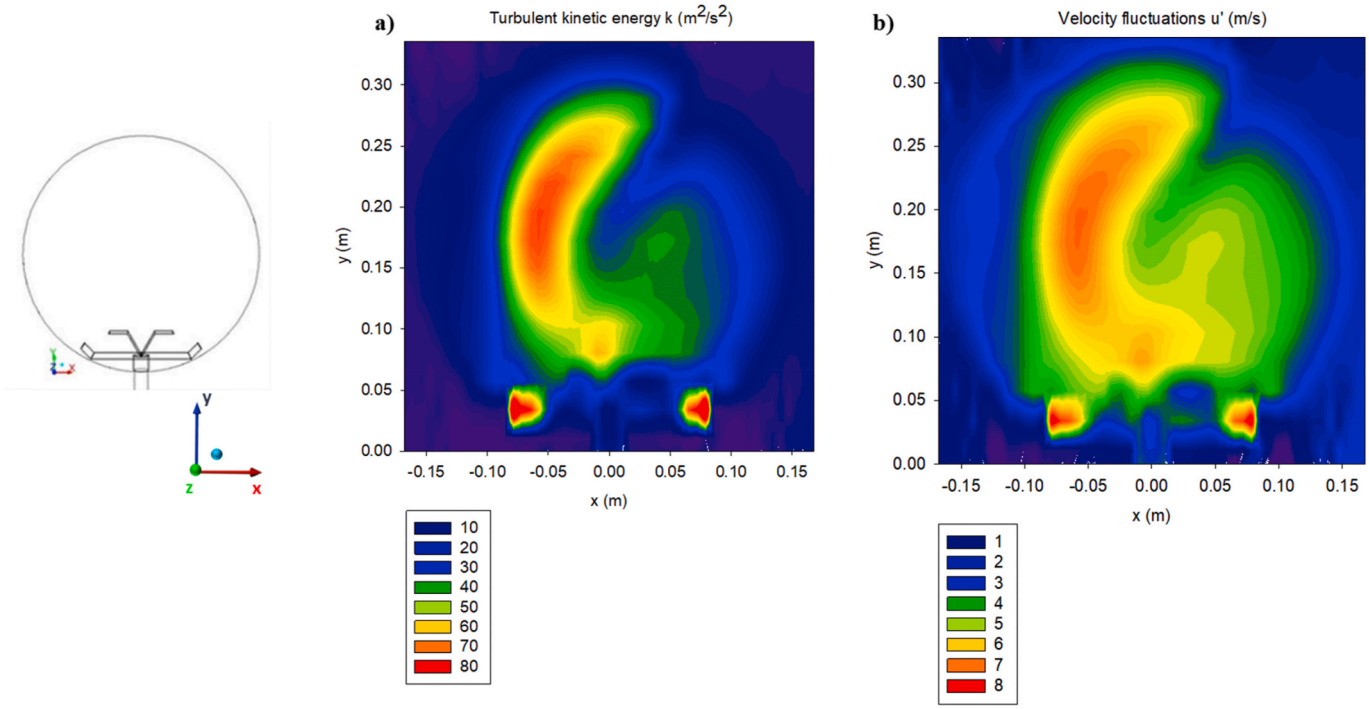

Fig. 1. Maps of the turbulent kinetic energy k (a) and of the velocity fluctuations, u' (b), C_{dust} = 200 g/m^3, V = 20 L, (x–y) plane.

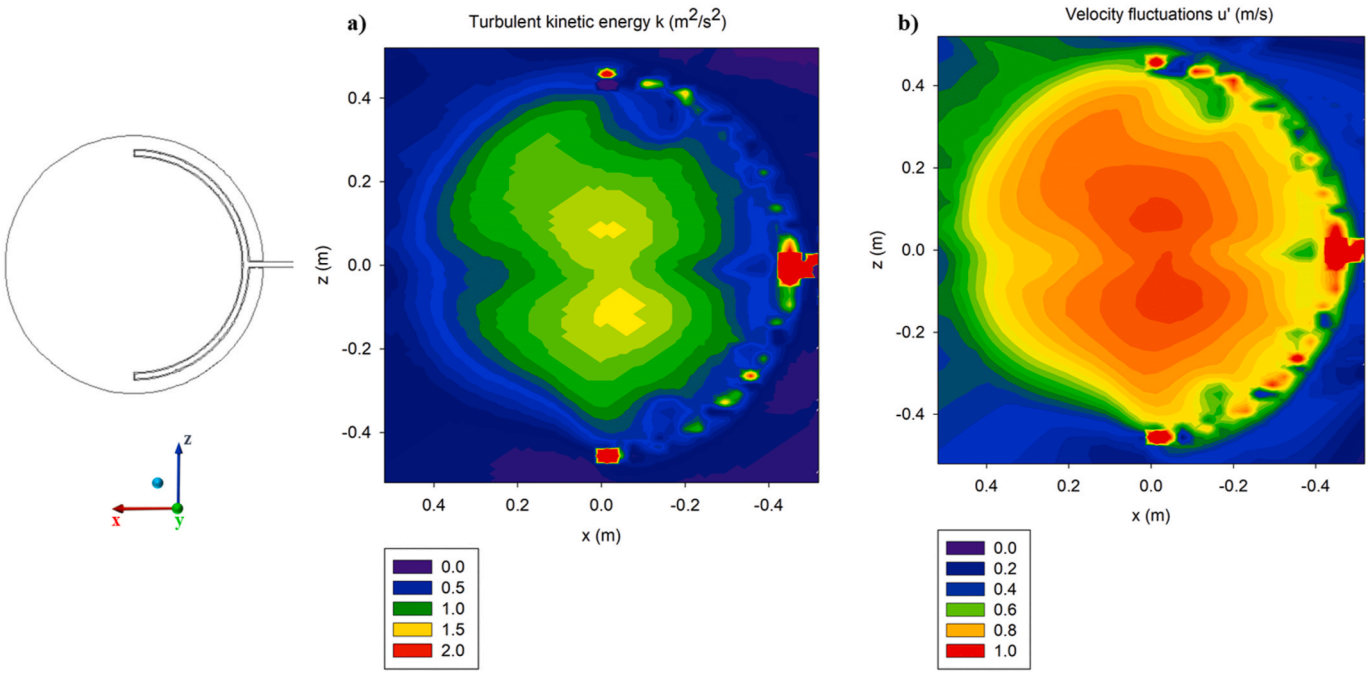

Fig. 2. Map of the turbulent kinetic energy, k (a) and of the velocity fluctuations, u' (b), C_{dust} = 200 g/m^3, V = 1 m^3, (x–z) plane.

the volatiles coming from the dust pyrolysis. Starting from each volatile composition, we performed the simulation of the flame propagation by means of the software CHEMKIN, evaluating the laminar burning velocity (S_l) (Reaction Design: San Diego, 2019). The amount and composition of the volatiles produced by the pyrolysis of cornstarch were obtained by the literature (Mazurkiewicz et al., 1993). In particular, in this work, the thermal decomposition products of the cornstarch are reported at two temperatures 450 °C and 550 °C. In Table 1, the literature data are given at 450 °C and 550 °C. Starting from the composition given in Table 1, we computed the volatile amount and composition at varying the dust concentration in the vessel. Volatile matter was determined equal to 80%wt of the dried sample initial weight by measuring the weight loss when heated up to 1000 °C at 10 °C/min (N_2 flow) in a Simultaneous Thermal Analyzer TG/DSC (TA Instrument Q600SDT). In Tables 2 and 3 the data are given for the 20 L and 1 m^3 vessel, respectively.

In Fig. 3, the laminar burning velocity obtained by CHEMKIN simulations are shown starting from the volatile compositions at 450 °C and 550 °C. Literature data obtained with different experimental rigs, granulometries and concentration are also reported. Proust and Veyssiere (1988) observed and evaluated the flame propagation of cornstarch-air mixtures (mean diameter 20 μm, concentration 100–220 g/m^3) within a 3 m long tube where the dust dispersion was realized though the elutriation above a fluidized bed (Proust and Veyssiere, 1988). Proust (1993) assessed S_l within a 1.5 m long tube where the dust dispersion was realized though the elutriation above a fluidized bed for starch dust-air mixtures, lycopodium-air mixtures and sulphur flower-air mixtures (mean particle diameter 25–45 μm, concentration 100–300 g/m^3) through the tube and direct methods (Proust, 1993). Nagy and Verakis (1983) derived laminar burning velocities and the deflagration index for clouds at 500 g/m^3 in concentration in air of various dusts through experimental dust explosion data from the elongated 1.2 L Hartmann bomb (Nagy and Verakis, 1983). Mazurkiewicz et al. (1993) measured the laminar burning velocity of cornstarch-air flames (mean particle diameter 15 μm, concentration 500 g/m^3) in a vertical 50 × 50 mm square tube, 1 m long, where the suspension was generated through elutriation of dust particles above a fluidized bed (Mazurkiewicz et al., 1993).

van Wingerden and Stavseng (1996) measured the laminar burning velocity of cornstarch-air and maize starch-air flames (mean particle diameter <100 μm, concentration 80–200 g/m^3 and 45–300 g/m^3, respectively) in an 1.6 m long vertical tube made of transparent

Table 1
Volatiles produced by the pyrolysis of cornstarch (Mazurkiewicz et al., 1993).

Gaseous species	450 °C	550 °C
H_2 (%)	0.86	4.82
CO (%)	42.73	39.06
CH_4 (%)	18.27	25.05
CO_2 (%)	38.13	31.06

Table 2
Volatiles produced by the pyrolysis of cornstarch, oxygen and nitrogen in the 20 L and 1 m^3 vessels, at varying the dust concentration at 450 °C. The stoichiometric oxygen amount is also shown.

C (g/m^3)	H_2 (%)	O_2 (%)	N_2 (%)	CO (%)	CH_4 (%)	CO_2 (%)	$O_{2,stoich}$ (%)
400	0.17	16.84	63.36	8.46	3.62	7.55	11.55
500	0.20	16.05	60.37	10.08	4.31	8.99	13.76
600	0.23	15.33	57.66	11.55	4.94	10.30	15.76
700	0.26	14.67	55.17	12.89	5.51	11.50	17.60
800	0.29	14.06	52.89	14.12	6.04	12.60	19.28
900	0.31	13.50	50.79	15.26	6.52	13.61	20.83

Table 3
Volatiles produced by the pyrolysis of cornstarch, oxygen and nitrogen in the 20 L and 1 m^3 vessels, at varying the dust concentration at 550 °C. The stoichiometric oxygen amount is also shown.

C (g/m^3)	H_2 (%)	O_2 (%)	N_2 (%)	CO (%)	CH_4 (%)	CO_2 (%)	$O_{2,stoich}$ (%)
200	0.58	18.48	69.53	4.68	3.00	3.72	8.64
300	0.82	17.44	65.60	6.63	4.25	5.27	12.22
400	1.03	16.51	62.09	8.36	5.36	6.65	15.43
500	1.23	15.67	58.93	9.92	6.37	7.89	18.30
600	1.40	14.91	56.09	11.33	7.27	9.01	20.90
700	1.56	14.22	53.50	12.61	8.09	10.03	23.26

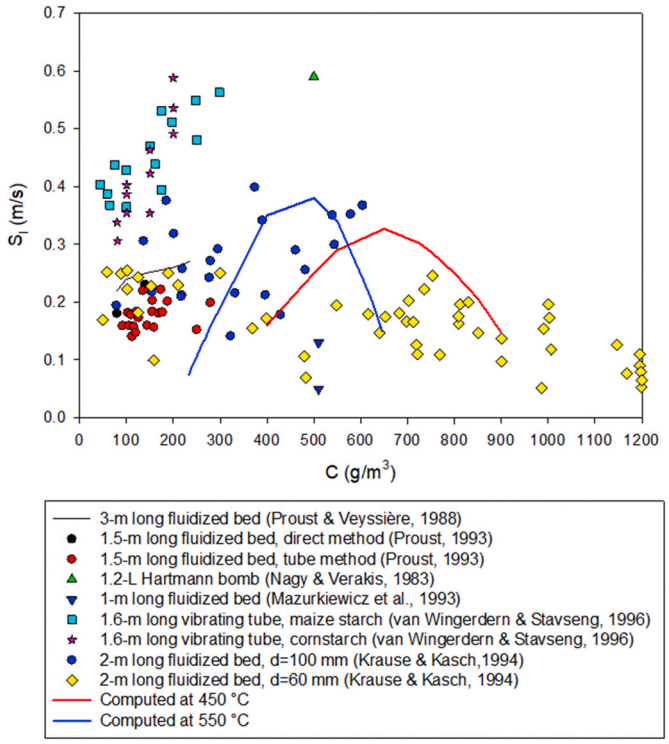

Fig. 3. Laminar burning velocity as function of the dust concentration as computed at pyrolysis temperature: 450 °C and 550 °C. Literature data are also shown.

polycarbonate where the dust was supplied continuously into the top of the tube from a horizontally vibrating sieve and a vibratory dust feeder (van Wingerden and Stavseng, 1996). The burning velocity in laminar flows was studied in a vertical cylindrical tube of 2 m in length and 300 mm in diameter where dust was layered on a porous filter plate and elutriated in a fluidized bed at the beginning of each experiment by Krause and Kasch (1994) (Krause and Kasch, 1994). From the data shown in Fig. 3, it appears that a very good agreement is obtained with the data provided by Krause and Kasch (1994) (Krause and Kasch, 1994).

2.3. Pressure/time history

To evaluate the pressure time history, the equation of Dahoe (Dahoe et al., 1996) has been used:

$$r_f = R_{vessel}\left[1-\left(\frac{P_0}{P}\right)^{\frac{1}{\gamma}}\frac{P_{MAX}-P}{P_{MAX}-P_0}\right]^{\frac{1}{3}} \quad (3)$$

where r_f (m) is the flame radius, R_{vessel} (m) is the vessel radius, P_0 (bar) is the initial pressure, P (bar) is the pressure and γ (−) is the heat capacity ratio. In Equation (3), P_{max} is the maximum pressure which was calculated by means of GASEQ software (Morley, 2005).

At each radius value which corresponds to the flame position, the corresponding pressure has been calculated. To evaluate the flame position (r_f) as function of time, we used the turbulent burning velocity (S_t):

$$t = \frac{r}{S_t} \quad (4)$$

Once obtained the pressure-time history, the deflagration index can be calculated through the cubic relationship (Equation (5))

$$K_{St} = \left(\frac{dP}{dt}\right)_{max} V^{1/3} \quad (5)$$

where $\left(\frac{dP}{dt}\right)_{max}$ (bar/s) is the maximum rate of pressure rise and V (m^3) is the vessel volume.

3. Results

3.1. Explosion parameters: 20 L vessel

Fig. 4 shows the radial profile of the turbulent kinetic energy (k) as computed at 60 ms which is the ignition delay time according to the standard in the 20 L vessel (ASTM E1226-19, 2019). The turbulent kinetic energy significantly varies along the radius, reaching a maximum at r = 0.04 m.

The evaluation of the pressure histories has been performed at three different conditions:

1) CASE 1: implementing the radial profile of turbulent kinetic energy
2) CASE 2: assuming the turbulent kinetic energy as constant and equal to the maximum value
3) CASE 3: assuming the turbulent kinetic energy as constant and equal to the minimum value.

Fig. 5 shows the pressure histories as obtained varying the dust concentration in the 20 L vessel at two pyrolysis temperature values (450 °C, top; 550 °C, bottom). The pressure histories have calculated assuming the turbulent kinetic energy varies along the radius as obtained by the CFD simulations (CASE 1).

From the profiles of Fig. 5, we calculated the maximum rate of pressure rise and then the deflagration index (Equation (5)). In Fig. 6 the maximum pressure (top) and the deflagration index (bottom) are plotted as function of the nominal dust concentration, as obtained by using the pyrolysis data at 450 °C and 550 °C.

At the two pyrolysis temperatures, the maximum values of K_{St} are almost similar: 238 bar m/s at 550 °C and 223 bar/m s at 450 °C. In both cases, the dust is classified as St-2 (200< K_{st} <300).

The maximum value of P_{max} is slightly higher when pyrolysis occurs at 550 °C (8 bar) than at 450 °C (7.6 bar). The dust concentration at which the $K_{St,max}$ and P_{max} are attained changes as function of

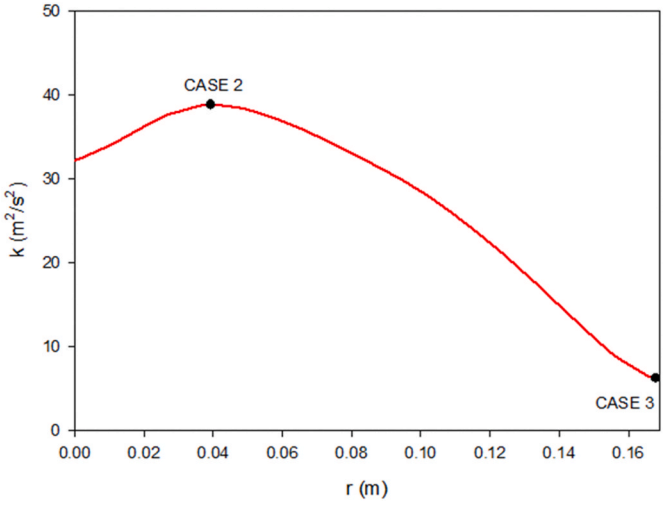

Fig. 4. Turbulent kinetic energy as function of the radial position in the 20 L vessel as computed at 60 ms

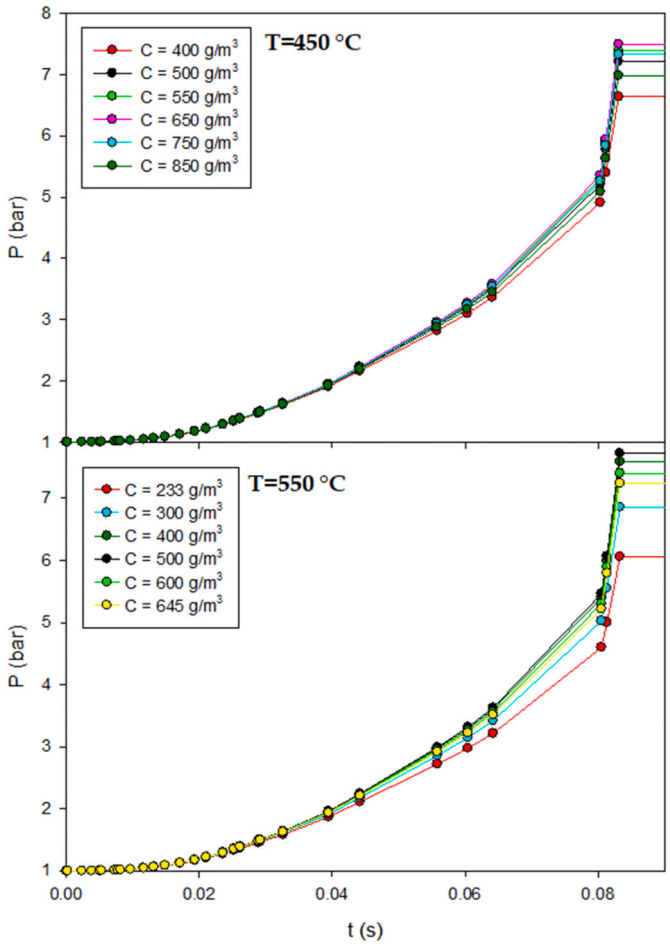

Fig. 5. Pressure time histories as function of time at different dust concentration and pyrolysis temperature (top: 450 °C; bottom: 550 °C) calculated in the 20 L vessel; CASE 1.

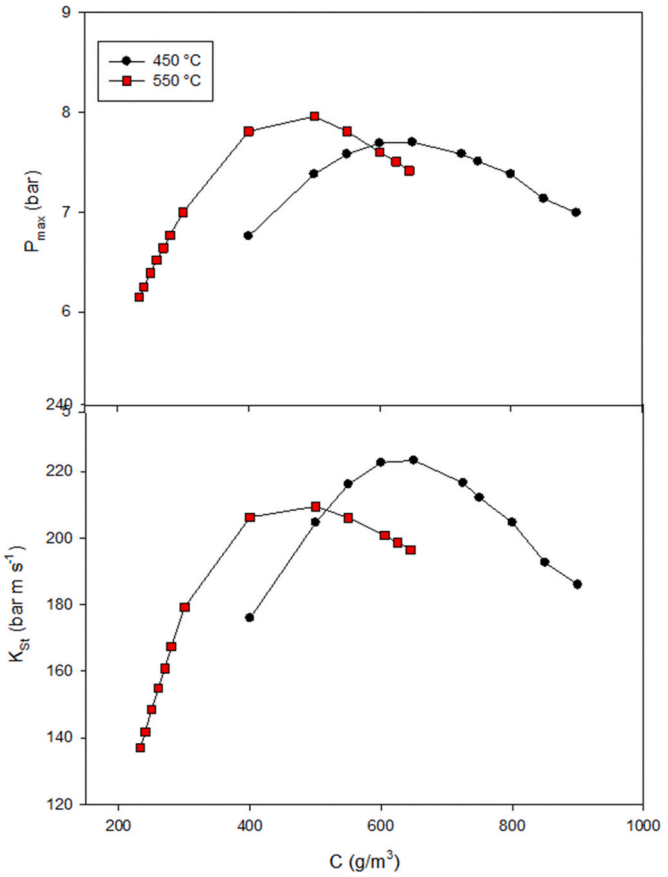

Fig. 6. Maximum pressure (P_{max}, top) and deflagration index (K_{St}, bottom) as function of nominal dust concentration as calculated at two pyrolysis temperature values (450 °C and 550 °C), CASE 1.

temperature: C = 500 g/m^3 at 550 °C and at C = 725 g/m^3 at 450 °C.

Calculations of the deflagration index were also performed by assuming *u'* corresponding to the maximum value simulated inside the 20 L vessel (CASE 2). In Fig. S1 the pressure time histories plotted as function of time, as calculated at different nominal dust concentration and pyrolysis temperature (450 °C and 550 °C). From the pressure temporal profiles, we calculated the deflagration index and the maximum pressure. In Fig. S2 the maximum pressure (top) and the deflagration index (bottom) are plotted as function of the nominal dust concentration, as obtained by using the pyrolysis data at 450 °C and 550 °C. In this case, the values are much higher, and the dust would be classified as St-3. At the two pyrolysis temperatures, the maximum values of K_{St} are almost similar: 540 bar m/s at 550 °C and 527 bar/m s at 450 °C. The maximum value of P_{max} is slightly higher when pyrolysis occurs at 550 °C (7.96 bar) than at 450 °C (7.7 bar). The dust concentration at which the $K_{St,max}$ and P_{max} are attained changes as function of temperature: C = 500 g/m^3 at 550 °C and at C = 650 g/m^3 at 450 °C.

In Fig. S3 the pressure time histories are as calculated at different nominal dust concentration and pyrolysis temperature (450 °C, top and 550 °C, bottom) in the case of minimum turbulence (CASE 3). From the temporal profiles of figure, we calculated the deflagration index and the maximum pressure. In Fig. S4 the maximum pressure (top) and the deflagration index (bottom) are plotted versus the nominal dust concentration at the two temperature values. In this case, the effect of the pyrolysis temperature is more significant. This result is related to the major role of the mixture reactivity with respect to the turbulence level. The maximum values of K_{St} are 50 bar m/s at 550 °C and 35 bar/m s at 450 °C. In both cases, the dust is classified as St-1. The maximum value of P_{max} is slightly higher when pyrolysis occurs at 550 °C (8 bar) than at 450 °C (7.6 bar). It is worth noting that the value of P_{max} does not depend on the fluid flow conditions. The dust concentration at which the $K_{St,max}$ and P_{max} are attained changes as function of temperature: C = 500 g/m^3 at 550 °C and at C = 650 g/m^3 at 450 °C.

In Fig. 7, the deflagration index as calculated at different fluid flow conditions (CASE 1, CASE 2 and CASE 3) and at two temperature values (450 °C, top and 550 °C, bottom), are shown together with the literature data. Eckhoff and Mathisen (1978) investigated the influence of moisture of 37 μm starch grains on the rate of pressure rise during explosions in a 1.2 L Hartmann bomb at 500, 1000 and 2000 g/m^3 (Eckhoff and Mathisen, 1978). Nagy and Verakis (1983) investigated the influence of moisture of starch grains on the rate of pressure rise during explosions in a 1.2 L Hartmann bomb at 500 g/m^3 (Nagy and Verakis, 1983). Table E.1(a) of the NFPA 68, Guide for Venting of Deflagrations, 2002 Edition shows the deflagration index result in the 1 m^3 vessel for cornstarch with mean diameter and concentration equal to 7 μm and 230 g/m^3 respectively (National Fire Protection Association, 2004). Proust (1993) determined the explosion parameters of cornstarch-air mixtures with mean diameter and concentration equal to 28 μm and 233 g/m^3 respectively in the 20 L vessel (Proust, 1993). The best agreement is obtained at pyrolysis temperature equal to 450 °C and laminar (CASE 3) and/or variable turbulence conditions (CASE 1). It is worth noting that in our calculations the effect of variable concentration along the radius has not been taken into account. Calculations have been performed by

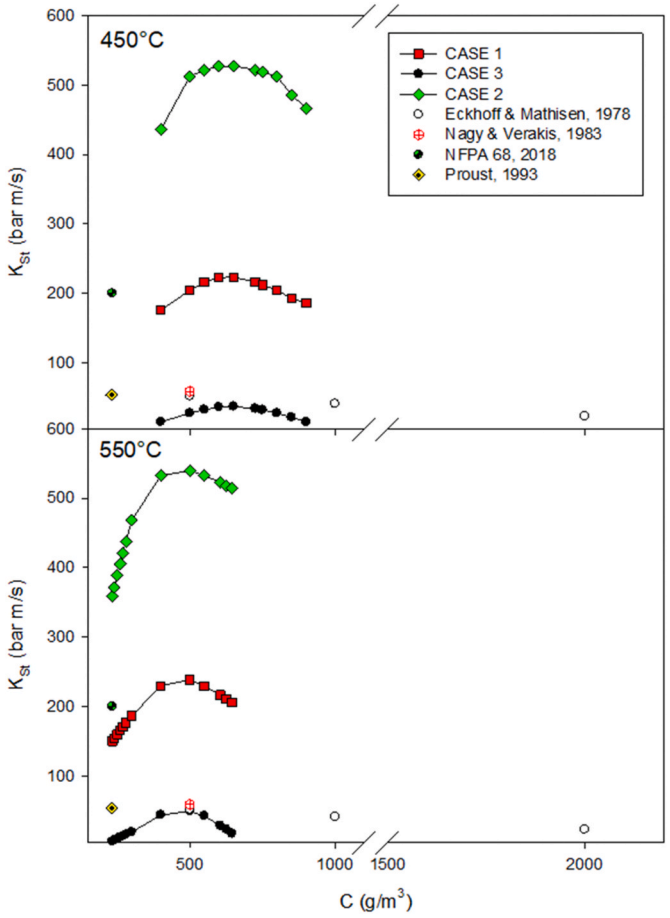

Fig. 7. Deflagration index as function of nominal dust concentration as calculated at different fluid dynamic conditions, at pyrolysis temperature equal to 450 °C (top) and 550 °C (bottom). Literature data are also shown.

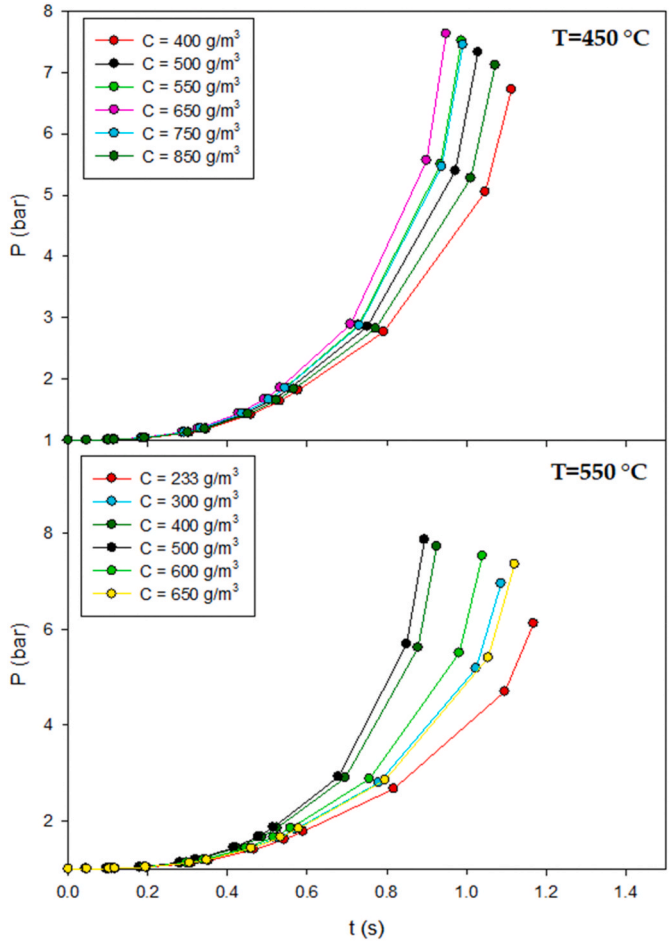

Fig. 8. Pressure time histories as function of time at different dust concentration and pyrolysis temperature (top: 450 °C; bottom: 550 °C) calculated in the 1 m^3 vessel, CASE 1.

assuming constant dust concentration (i.e., constant laminar burning velocity within the vessel) and equal to the nominal value.

3.2. Explosion parameters: 1 m^3 vessel

Pressure-time histories have been calculated as function of time, at different pyrolysis temperature values (450 °C, top and 550 °C, bottom) and different nominal dust concentrations. As in the case of the 20 L vessel, calculations were performed at different initial conditions: variable turbulence (CASE 1), maximum turbulence (CASE 2) and laminar (CASE 3). From the temporal trend of pressure, the maximum rate of pressure rise and the maximum pressure have been calculated.

In Fig. 8 the pressure histories as obtained at varying the dust concentration in the 1 m^3 vessel at two temperature values (450 °C, top; 550 °C, bottom) are shown. The pressure histories have calculated assuming the turbulent kinetic energy variable along the radius as obtained by the CFD simulations (CASE 1). From the values of the rate of pressure rise it has been possible to calculate the deflagration index as a function of the dust concentration.

In Fig. 9 the maximum pressure (top) and the deflagration index (bottom) are plotted versus the nominal dust concentration at the two temperature values. The maximum value of K_{St} ($K_{St\ max}$) is attained at different dust concentration but the values are almost similar: 16.3 bar m/s at 550 °C and 14 bar m/s at 450 °C. In both cases, the dust is classified as St-1. The maximum values are attained at C = 500 g/m^3 at 550 °C and at C = 650 g/m^3 at 450 °C. The maximum pressure is attained at C = 500 g/m^3 at 550 °C and at C = 725 g/m^3 at 450 °C.

In Fig. S5 the computed temporal histories of pressure are shown, at different nominal dust concentration and at 450 °C (top) and 550 °C (bottom), assuming the turbulent kinetic energy uniform and equal to the maximum value attained in the vessel (CASE 2).

From the values of the rate of pressure rise it has been possible to calculate the deflagration index as a function of the dust concentration. In Fig. S6 the maximum attained pressure (top) and the deflagration index (bottom) are plotted versus the nominal dust concentration, as obtained by using the pyrolysis data at 450 °C and 550 °C. The maximum value of K_{St} ($K_{St\ max}$) is attained at different dust concentration but the values are almost similar: 43 bar m/s at 550 °C and 39 bar/m s at 450 °C. In both cases, the dust is classified as St-1. The maximum values are attained at C = 500 g/m^3 at 550 °C and at C = 725 g/m^3 at 450 °C.

In order to quantify the effect of the spatial variation of turbulence on the explosion parameters, we performed the calculation also assuming a uniform value of the turbulence intensity. In the following figures, we report the results obtained by assuming that the turbulence level is negligible thus simulating a laminar flame propagation (CASE 3).

In Fig. S7 the computed temporal histories of pressure are shown, at different nominal dust concentration and at 450 °C (top) and 550 °C (bottom). From the values of the rate of pressure rise it has been possible to calculate the deflagration index as a function of the dust concentration. In Fig. S8 the maximum attained pressure (top) and the deflagration index (bottom) are plotted versus the nominal dust concentration,

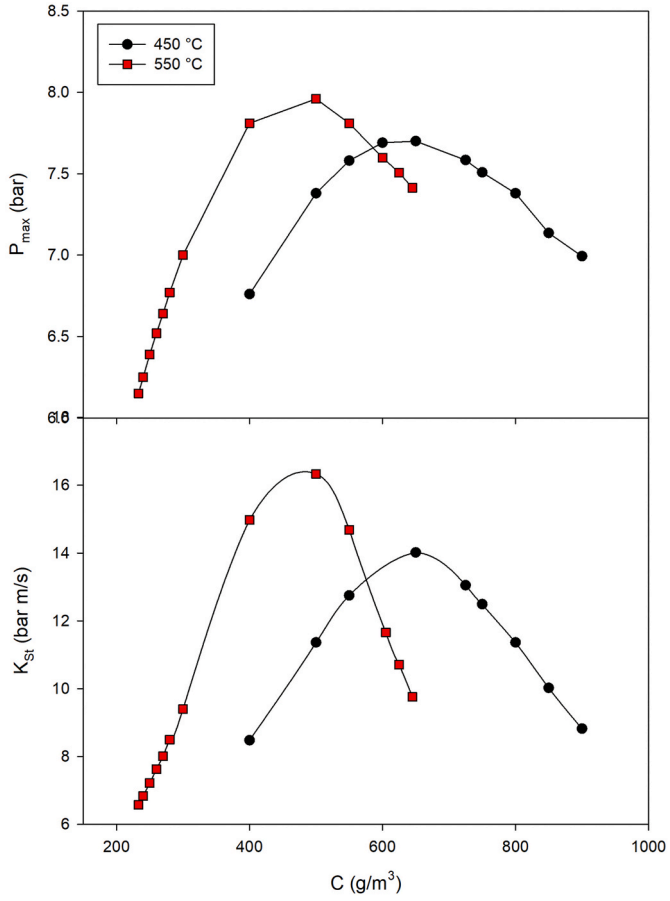

Fig. 9. Maximum pressure (P_{max}, top) and deflagration index (K_{St}, bottom) as function of nominal dust concentration as calculated at two pyrolysis temperature values (450 °C and 550 °C), 1 m^3 vessel, CASE 1.

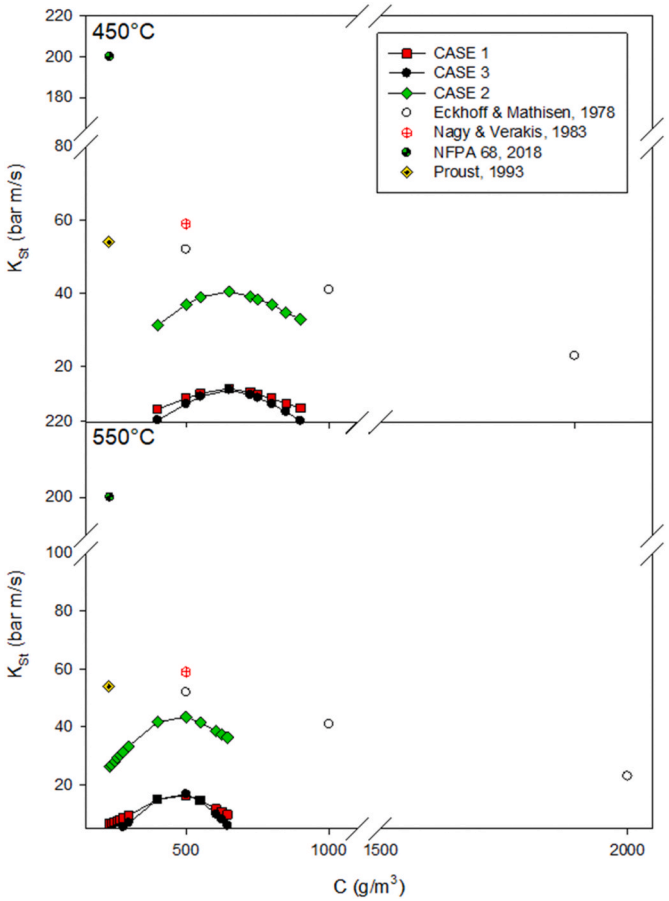

Fig. 10. Deflagration index as function of nominal dust concentration as calculated at different fluid dynamic conditions (CASE 1, 2 and 3), at pyrolysis temperature equal to 450 °C (top) and 550 °C (bottom), 1 m^3 vessel. Literature data are also shown.

as obtained by using the pyrolysis data at 450 °C and 550 °C. The trend is almost similar to that relative to the CASE 1. The maximum value of K_{St} ($K_{St\ max}$) is attained at different dust concentration but the values are almost similar: 16.3 bar m/s at 550 °C and 14 bar m/s at 450 °C. In both cases, the dust is classified as St-1. The maximum values are attained at C = 500 g/m^3 at 550 °C and at C = 650 g/m^3 at 450 °C. The maximum pressure is attained at C = 500 g/m^3 at 550 °C and at C = 725 g/m^3 at 450 °C.

In the following Fig. 10, the deflagration index as calculated in the 1 m^3 vessel at different fluid flow conditions (CASE 1, CASE 2 and CASE 3) and at two temperature values (450 °C, top and 550 °C, bottom), are shown together with the literature values. In the following figures, the deflagration index as calculated at laminar conditions, radially varying turbulence and turbulence value at the centre are shown. The best agreement is obtained in the case of turbulent conditions (CASE 2). It is worth noting that in our calculations the effect of variable concentration has not been considered. Calculations have been performed by assuming constant dust concentration and equal to the nominal value.

3.3. Comparison between 20 L and 1 m^3 vessels

The results of our calculations are summarised in the following tables.

The maximum values of K_{St} together with the corresponding dust concentration are given in Table 4 and in Table 5 for the 20 L and 1 m^3 vessels, respectively. It is found that the concentration corresponding to the maximum value of the deflagration index is the same in both vessels: C = 500 g/m^3 when the pyrolysis temperature is 450 °C and 650 g/m^3 when the pyrolysis temperature is 550 °C. The main difference lies in the values of the maximum deflagration index. In the case of the 20L vessel, the dust is classified St-2 and St-3 in the presence of turbulence (CASE 1 and CASE 2), while St-1 in the case of laminar (CASE 3) conditions. Conversely, in the 1 m^3 vessel, the class is always St-1.

The variability of turbulence in the 20 L vessel is much more significant than in the 1 m^3 and consequently the variability of the K_{St} is much higher. In Fig. 11 the K_{St} values are shown together with the deviation from the average value. It clearly appears that the variability of the turbulence level inside the vessels and then on the deflagration index is higher in the 20 L vessel than in the 1 m^3 vessel. As a consequence, the repeatability of the measurements of K_{St} is much higher in the 1 m^3 vessel than in the 20 L vessel. Indeed, in the 1 m^3 vessel, the turbulence level is relatively low and almost uniform in space. Consequently, quasi laminar conditions stablish. At quasi-laminar conditions, the tests of combustible dusts are less susceptible to turbulence variations due to different dust properties like dust density, size and shape.

Conversely, in the case of the 20 L vessel, the turbulence level is highly non-uniform in space, and its value is very high. The spatial turbulence level variation is much wider than that in the 1 m^3 vessel. Therefore, every parameter which may affect turbulence (like dust properties) may have a great impact on the test result. In this sense, the evaluations in the 1 m^3 sphere are more reliable and repeatable, less dependent on the properties of the dust in question.

Immediately after the dust dispersion inside the test vessel, turbulence builds up and starts decreasing. Consequently, the turbulence level at moment of ignition significantly depends on the ignition delay time t_d. According to the standard procedure, measurements of the deflagration

Table 4
Maximum values of K_{St} as calculated at two pyrolysis temperatures (450 °C and 550 °C), 20 L vessel.

T = 550 °C				T = 450 °C		
C (g/m^3)	$K_{St,max}$ (bar m/s)	Class		C (g/m^3)	$K_{St,max}$ (bar m/s)	Class
500	540	St-3	CASE 2	650	527	St-3
500	238	St-2	CASE 1	650	223	St-2
500	49	St-1	CASE 3	650	37	St-1

Table 5
Maximum values of K_{St} as calculated at two pyrolysis temperatures (450 °C and 550 °C), 1 m^3 vessel.

T = 550 °C				T = 450 °C		
C (g/m^3)	$K_{St,max}$ (bar m/s)	Class		C (g/m^3)	$K_{St,max}$ (bar m/s)	Class
500	43	St-1	CASE 2	650	40	St-1
500	16	St-1	CASE 1	650	14	St-1
500	17	St-1	CASE 3	650	14	St-1

index in the two vessels may be considered as equivalent if the ignition delay times are properly chosen. The ignition delay time should be (60 ± 5) ms in the 20 L vessel and (600 ± 100) ms in the 1 m^3 vessel. However, when comparing the results obtained at these values of the ignition delay time, the turbulence level and consequently the deflagration index in the 20 L vessel are much higher than those obtained in the 1 m^3. We then performed calculations at increasing the ignition delay time in the 20 L vessel, to find the conditions at which the spatial-temporal distribution of turbulence is equivalent. From the CFD simulations, we obtained the turbulent kinetic energy as function of time and space in the 20 L vessel. In Fig. 12 the turbulent kinetic energy as calculated at the centre of the vessel is plotted versus the ignition delay time (t_d). The black line represents the turbulent kinetic energy in the centre of the 1 m^3 vessel, at t_d = 600 ms. It appears that only at 260 ms, the turbulent kinetic energy in the 20 L vessel is equal to that attained in the 1 m^3 vessel. In Fig. 13, the spatial profile of the turbulent kinetic energy (k) is plotted as function of the radius inside the 20 L vessel, at different values of the ignition delay time. It can be concluded that on increasing the ignition delay time, the turbulent kinetic energy profile becomes flattener and more homogeneous.

Starting from the pressure temporal profiles, we calculated the deflagration index at different values of the ignition delay time. In Fig. 14 the values of the maximum deflagration index are plotted versus the ignition delay time. The error bars represent the values obtained by assuming the fluid flow uniform and equal to laminar conditions (CASE 3, minimum) and fully turbulent conditions (CASE 2) at the maximum value. The values of K_{St} computed in the 1 m^3 vessel in the CASE 2 and CASE 3 are also shown. It is worth noting that on increasing the ignition delay time, the deflagration index calculated in the 20 L vessel decreases, reaching the values obtained in the 1 m^3 vessel. It is also noting that the deviation from the average value decreases as a result of the more uniform turbulent kinetic energy profile.

The different values measured of the explosion parameters in the two standard vessels derive from the different turbulence level which significantly affect the flame propagation. Depending on the flame burning rate and the turbulence level, the interaction between the flame front and the eddies significantly changes, thus leading to turbulent combustion regimes. Depending on the flame laminar burning velocity S_l, the flame thickness (l_F), the turbulent fluctuations (u') and the vessel scale (R_{vessel}), different combustion regimes have been identified in the Borghi diagram (Abdel-Gayed and Bradley, 1989; Borghi, 1985; Peters, 1986; Poinsot, 1990). Starting from the data obtained by our simulations, we evaluated the combustion regime by changing the vessel scale (20 L, 1 m^3) and the nozzle (rebound, perforated annular). In Table 6 the values of all the parameters and numbers are given as calculated for all the configurations under study.

In Fig. 15, the Borghi diagram with the indication of the combustion regime for each configuration is shown. The turbulence level in the 20 L sphere, is always higher than that in the 1 m^3 vessel, leading to the generation of a flame propagation in the thin reaction zone, whatever

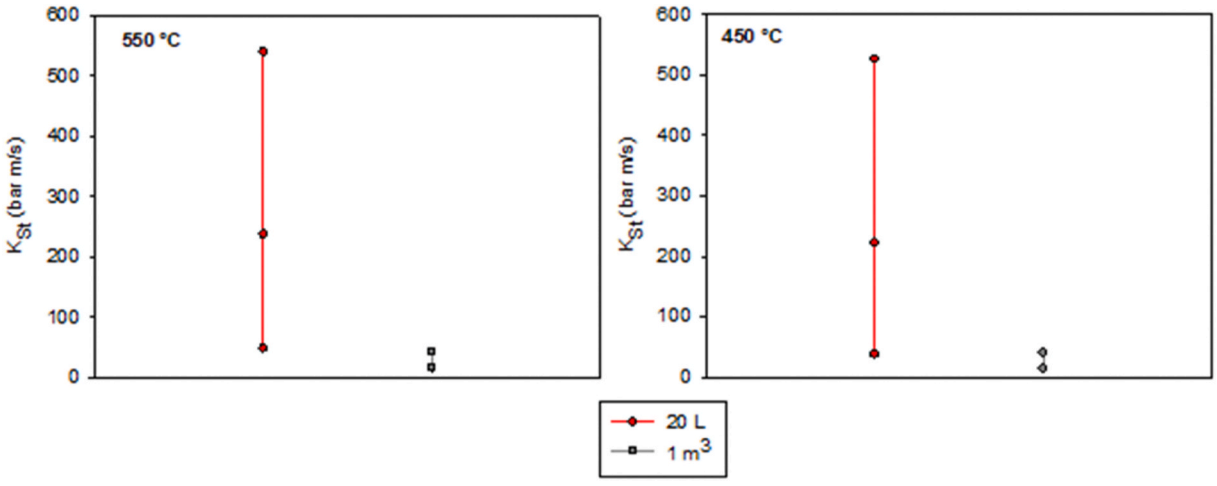

Fig. 11. K_{st} calculated in the 20 L and 1 m^3 vessels together with the deviation, at 450 °C and 550 °C.

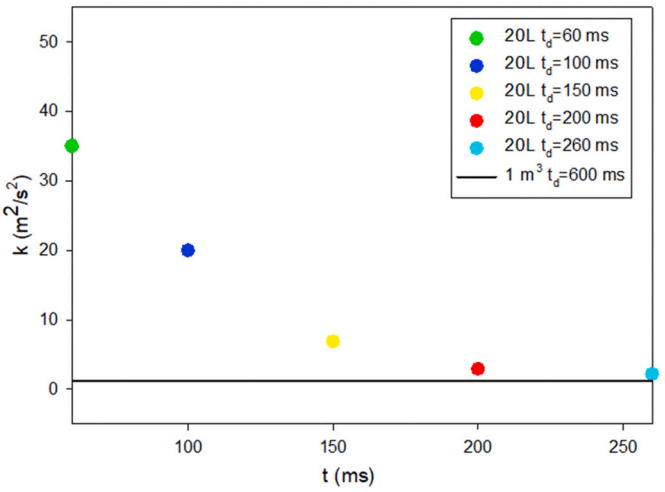

Fig. 12. Turbulent kinetic energy as function of the ignition delay time in the centre of the 20 L vessel. Black line is the value obtained in the 1 m^3 vessel.

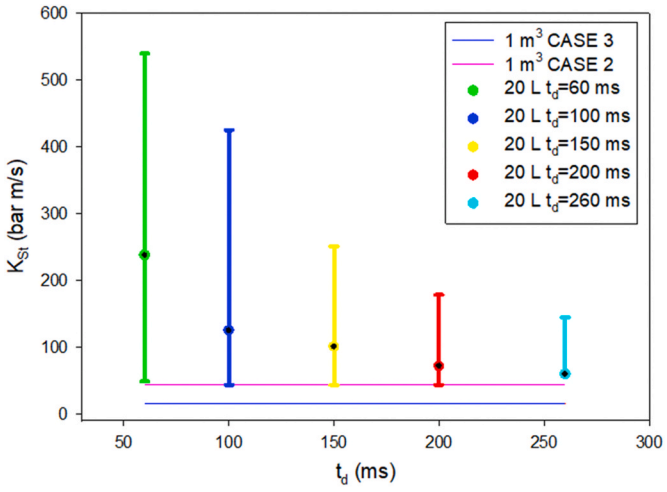

Fig. 14. Deflagration index and its deviation as function of the ignition delay time, V = 20 L. Red and blue lines are the value obtained in the 1 m^3 vessel for the CASE 2 and CASE 3, respectively. (For interpretation of the references to colour in this figure legend, the reader is referred to the Web version of this article.)

the nozzle used. In the thin reaction zones regime, the Kolmorogov scale becomes smaller than the flame thickness, which implies Ka>1. Turbulence then increases the transport within the preheating region. Moreover, mixing is enhanced at higher Ka numbers, which leads to higher volumetric heat release and shorter combustion times.

Conversely, in the 1 m^3 vessel, the corrugated flamelets regime is established. In the corrugated flamelet regime, the laminar flame thickness is smaller than the Kolmogorov scale, and hence Ka<1. Turbulence will therefore wrinkle the flame but will not enters in the laminar flame structure (the flow is quasi laminar). The same turbulent flame regime is established when in the 20 L vessel the ignition delay time is equal to 260 ms.

As a main conclusion, the difference between the explosion tests in the 20 L and 1 m^3 vessels, are qualitative other than quantitative being not only the turbulent kinetic energy different but also the turbulent combustion regime which significantly affects the flame propagation mode and eventually the explosion severity.

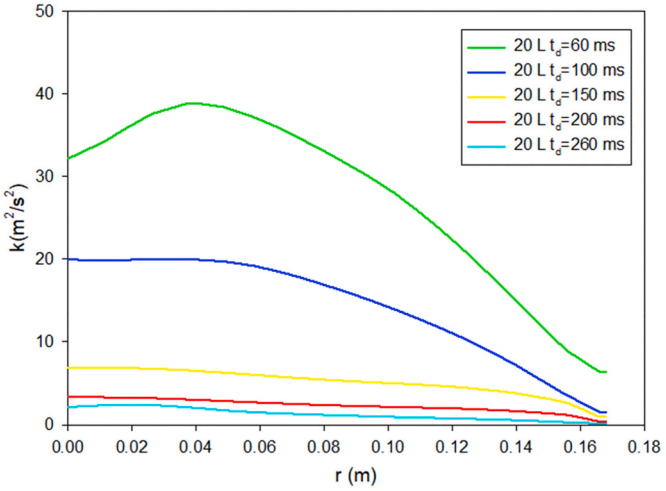

Fig. 13. Turbulent kinetic energy as function of the radius at different values of the ignition delay time, V = 20 L.

4. Conclusions

The role of turbulence on the explosion parameters (maximum pressure and deflagration index) in terms of level and spatial distribution was quantified in both 20 L and 1 m^3 vessels by means of CFD simulations. The computed maps show significant spatial variation of the turbulent kinetic energy in the 20 L vessel. Conversely, in the 1 m^3 vessel, the turbulence level is much more uniform. The value of the turbulent kinetic energy computed at the ignition delay time (60 ms in the 20 L and 600 ms in the 1 m^3 vessel) is much higher in the smaller vessel. Accordingly, by taking into account only the turbulence effect, we found that the computed value of the deflagration index is much higher in the case of the 20 L vessel. Cornstarch which is classified as St-1 in the 1 m^3 vessel, is classified St-1 or St-2 or St-3 in the 20 L sphere, depending on if uniform maximum or variable values of the turbulent kinetic are assumed. In order to get agreement between the data calculated in the two vessels, a more uniform turbulence level in the smaller vessel, less dependent on the size, shape, density and concentration of the dust, is mandatory. CFD simulations performed at varying the ignition delay time in the 20 L, suggest that the turbulent kinetic energy profile is much more uniform and similar to that of 1 m^3 vessel at ignition delay time equal to 260 ms. As a consequence, on increasing the ignition delay time, the deflagration index calculated in the 20 L vessel decreases reaching the values obtained in the 1 m^3 vessel. Therefore, an extension of the ignition delay time in the case of the 20 L vessel would lead to an improvement of the measurements in terms of reliability: once the dust is fixed (with its chemical nature), the evaluations would no longer be strongly influenced by diameter, concentration, shape, and humidity as the range of variation of the turbulence level and then the variability of the explosion parameters, would be narrower. Moreover, in this way, the explosion tests would be qualitatively and quantitatively similar in terms of initial level of turbulence and turbulent combustion regime.

Credit author statement

Maria Portarapillo: Methodology; Investigation; Writing - original draft. **Roberto Sanchirico:** Writing - Review & Editing. **Almerinda Di Benedetto:** Conceptualization; Writing - original draft; Supervision.

Table 6
Numbers of the Borghi diagram as calculated for all the configuration.

	S_l (max)	k (centre)	u' (centre)	l_F	u'/S_l	R_{vessel}/l_F	Ka	Re	Turbulent flame regime
20 L rebound (60 ms)	0.4	35	4.8	0.001	12	171.4	3.2	12076.1	thin reaction zone
20 L perforated (only air)	0.4	35	4.8	0.001	12.0	171.4	3.2	12076.1	thin reaction zone
20 L rebound (260 ms)	0.4	2.1	1.2	0.001	3.1	171.4	0.4	3175.4	corrugated flamelets
1 m^3 perforated (600 ms)	0.4	1.2	0.8	0.001	2.2	623.4	0.1	2236.0	corrugated flamelets

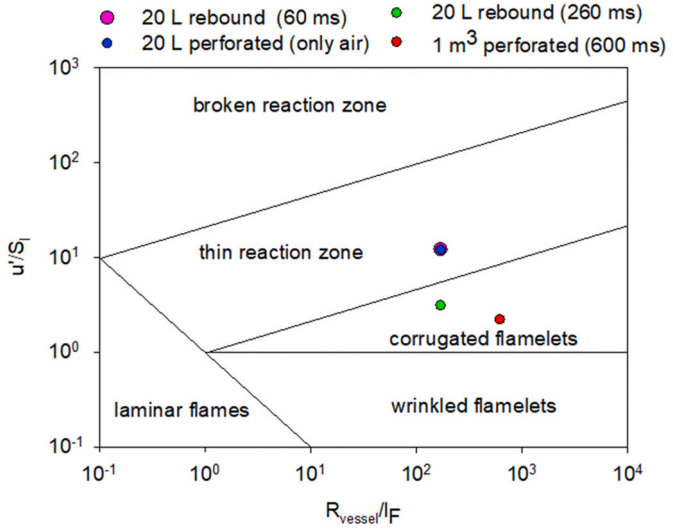

Fig. 15. Diagram of turbulent combustion regimes.

Declaration of competing interest

The authors declare that they have no known competing financial interests or personal relationships that could have appeared to influence the work reported in this paper.

Appendix A. Supplementary data

Supplementary data to this article can be found online at https://doi.org/10.1016/j.jlp.2021.104484.

References

Abdel-Gayed, R.G., Bradley, D., 1989. Combustion regimes and the straining of turbulent premixed flames. Combust. Flame 76, 213–218. https://doi.org/10.1163/187529293X00358.

ASTM E1226-19, 2019. Standard Test Method for Explosibility of Dust Clouds. ASTM Int. West Conshohocken, pp. 1–15. https://doi.org/10.1520/E1226-19.

ASTM E1515-14, 1993. Standard Test Method for Minimum Explosible Concentration of Combustible Dusts 1. ASTM Int. West Conshohocken, pp. 1–9. https://doi.org/10.1520/E1515-14.

ASTM E2931-13, 2013. Standard Test Method for Limiting Oxygen (Oxidant) Concentration of Combustible. ASTM Int. West, Conshohocken, PA. https://doi.org/10.1520/E2931-13.

Borghi, R., 1985. On the structure and morphology of turbulent premixed flames. In: Recent Advances in the Aerospace Sciences, pp. 117–138.

BS EN 14034-1, 2004. Determination of Explosion Characteristics of Dust Clouds Part 1: Determination of Maximum Pressure Pmax of Dust Clouds 3.

Cashdollar, K.L., Chatrathi, K., 1992. Minimum explosible dust concentrations measured in 20-L and 1-M3 chambers. Combust. Sci. Technol. 87, 157–171. https://doi.org/10.1080/00102209208947213.

Clouthier, M.P., Taveau, J.R., Dastidar, A.G., Morrison, L.S., Zalosh, R.G., Ripley, R.C., Khan, F.I., Amyotte, P.R., 2019. Iron and aluminum powder explosibility in 20-L and 1-m3 chambers. J. Loss Prev. Process. Ind. 62, 103927. https://doi.org/10.1016/J.JLP.2019.103927.

Dahoe, A.E., Cant, R.S., Scarlett, B., 2002. On the decay of turbulence in the 20-liter explosion sphere. Flow, Turbul. Combust. 67, 159–184. https://doi.org/10.1023/A:1015099110942.

Dahoe, A.E., Zevenbergen, J.F., Lemkowitz, S.M., Scarlett, B., 1996. Dust explosions in spherical vessels: the role of flame thickness in the validity of the "cube-root law. J. Loss Prev. Process. Ind. 9, 33–44. https://doi.org/10.1016/0950-4230(95)00054-2.

Di Benedetto, A., Garcia-Agreda, A., Russo, P., Sanchirico, R., 2012. Combined effect of ignition energy and initial turbulence on the explosion behavior of lean gas/dust-air mixtures. Ind. Eng. Chem. Res. 51, 7663–7670. https://doi.org/10.1021/ie201664a.

Di Benedetto, A., Russo, P., Sanchirico, R., Di Sarli, V., 2013. CFD simulations of turbulent fluid flow and dust dispersion in the 20 liter explosion vessel. AIChE 59, 2485–2496. https://doi.org/10.1002/aic.

Dust Safety Science, 2020. Combustible Dust Incident Database.

Eckhoff, R.K., Mathisen, K.P., 1978. A critical examination of the effect of dust moisture on the rate of pressure rise in Hartmann bomb tests. Fire Saf. J. 1, 273–280. https://doi.org/10.1016/0379-7112(78)90016-4.

Garcia Agreda, A., Di Benedetto, A., Russo, P., Salzano, E., Sanchirico, R., 2011. The role of ignition delay time on the deflagration index in a 20l bomb. Comput. Methods Appl. Mech. Eng. 57, 683–694.

Going, J.E., Chatrathi, K., Cashdollar, K.L., 2000. Flammability limit measurements for dusts in 20-L and 1-m3 vessels. J. Loss Prev. Process. Ind. 13, 209–219. https://doi.org/10.1016/S0950-4230(99)00043-1.

Hauert, F., Vogl, A., 1995. Measurement of Dust Cloud Characteristics in Industrial Plants (Number: PL 910695).

ISO 6184-1:1985, 1985. Explosion Protection Systems, Part 1, Determination of Explosion Indices of Combustible Dusts in Air.

Krause, U., Kasch, T., 1994. Investigations on burning velocities of dust/air mixtures in laminar flows. In: Oral Presentation.

Mazurkiewicz, J., Jarosinski, J., Wolanski, P., 1993. Investigations of burning properties of cornstarch dust-air flame. Arch. Combust. 13, 190–201.

Morley, C., 2005. GASEQ, a Chemical Equilibrium Program for Windows.

Nagy, J., Verakis, H.C., 1983. Development and Control of Dust Explosions.

National Fire Protection Association, 2004. NFPA 68, Guide for Venting of Deflagrations, p. 11, 2002 Edition 2002 Editi.

NFPA, N.68, 2018. Explosion Protection by Deflagration Venting.

Peters, N., 1986. Laminar flamelet concepts in turbulent combustion. In: 21th Symposium International on Combustion, pp. 1231–1250.

Pocheau, A., 1994. Scale invariance in turbulent front propagation. Phys. Rev. E 49, 1109–1122. https://doi.org/10.1103/PhysRevE.49.1109.

Poinsot, T.J., 1990. Direct Simulation of Turbulent Combustion.

Portarapillo, M., Trofa, M., Sanchirico, R., Di Benedetto, A., 2020. CFD simulations of dust dispersion in the 1 m3 explosion vessel. J. Loss Prev. Process. Ind. 68, 104274. https://doi.org/10.1016/j.jlp.2020.104274.

Proust, C., 1993. Experimental determination of the maximum flame temperatures and of the laminar burning velocities for some combustible dust-air mixtures. In: International Colloquium on Dust Explosions.

Proust, C., Accorsi, A., Dupont, L., 2007. Measuring the violence of dust explosions with the "20 l sphere" and with the standard "ISO 1 m3 vessel". Systematic comparison and analysis of the discrepancies. J. Loss Prev. Process. Ind. 20, 599–606. https://doi.org/10.1016/j.jlp.2007.04.032.

Proust, C., Veyssiere, B., 1988. Fundamental properties of flames propagating in starch dust-air mixtures. Combust. Sci. Technol. 62, 149–172. https://doi.org/10.1080/00102208808924007.

Pu, Y.K., Jarosinski, J., Johnson, V.G., Kauffman, C.W., 1991. Turbulence effects on dust explosions in the 20-liter spherical vessel. Symp. Combust. 23, 843–849. https://doi.org/10.1016/S0082-0784(06)80338-3.

Reaction Design: San Diego, 2019. CHEMKIN-PRO Release, 2019.

Rodgers, S.A., Ural, E.A., 2011. Practical issues with marginally explosible dusts—evaluating the real hazard. Process Saf. Prog. 30, 266–279. https://doi.org/10.1002/prs.

Taveau, J.R., Lemkowitz, S.M., Hochgreb, S., Roekaerts, D., 2018. Scaling up metal dusts deflagrations severity. In: Proceedings of the Twelfth International Symposium on Hazards, Prevention, and Mitigation of Industrial Explosions. Soesterberg, Netherlands.

Taveau, J.R., Lemkowitz, S.M., Hochgreb, S., Roekaerts, D.J.E.M., 2019. Metal dusts explosion hazards and protection. Chem. Eng. Trans. 77, 7–12. https://doi.org/10.3303/CET1977002.

van der Wel, P.G.J., van Veen, J.P.W., Lemkowitz, S.M., Scarlett, B., van Wingerden, C.J. M., 1992. An interpretation of dust explosion phenomena on the basis of time scales. Powder Technol. 71, 207–215. https://doi.org/10.1016/0032-5910(92)80010-T.

van Wingerden, K., Stavseng, L., 1996. Measurements of the laminar burning velocities in dust-air mixtures. VDI-Ber. 553–564.

Zhen, G., Leuckel, W., 1996. Determination of dust-dispersion-induced turbulence and its influence on dust explosions. Combust. Sci. Technol. 113–114, 629–639. https://doi.org/10.1080/00102209608935518.